ADVANCED ENERGY MATERIALS

www.advenergymat.de

Ternary Blended Fullerene-Free Polymer Solar Cells with 16.5% Efficiency Enabled with a Higher-LUMO-Level Acceptor to Improve Film Morphology

Kun Li, Yishi Wu, Yabing Tang, Ming-Ao Pan, Wei Ma,* Hongbing Fu, Chuanlang Zhan,* and Jiannian Yao*

Ternary approaches to solar cell design utilizing a small bandgap nonfullerene acceptor as the near infrared absorber to increase the short-circuit current density always decreases the open-circuit voltage. Herein, a highly efficient polymer solar cell with an impressive efficiency of 16.28 ± 0.20% enabled by an effective voltage-increased ternary blended fullerene-free material approach is reported. In this approach, the structural similarity between the host and the higher-LUMO-level guest enables the two acceptors to be synergized, obtaining increased open-circuit voltage and fill factor and a small increase of short-circuit current density. The same beneficial effects are demonstrated by using two host binary systems. The homogeneous fine film morphologies and the π–π stacking patterns of the host blend are well maintained, while larger donor and acceptor phases and increased lamellar crystallinity, increased charge mobilities, and reduced monomolecular recombination can be achieved upon addition of the guest nonfullerene acceptor. The increased charge mobilities and reduced monomolecular recombination not only contribute to the improved fill factor but also enable the best devices to be fabricated with a relatively thicker ternary blended active layer (110 vs 100 nm). This, combined with the absorption from the added guest acceptor, contribute to the increased short-circuit current.

1. Introduction

Due to the synthesis of highly efficient fused-ring electron acceptor (FREA) and the donor polymer materials,[1–12] bulk heterojunction fullerene-free polymer solar cells (PSCs) have achieved power conversion efficiencies (PCEs) greater than 15% in single-junction binary devices.[13,14] However, the performance of the binary system is still largely limited by the material's own properties (narrow absorption, small crystallinity, low charge mobility, strong recombination, etc.). In order to overcome these limitations, the strategy of adding a third component to the binary system, e.g., ternary solar cell approach, has come into being and shown wide-ranging applicability in improving the solar cell device function. The addition of a structurally similar third component can either extend the absorption range of solar emission spectrum, tune the frontier molecular orbital (FMOs) levels such as through forming homogeneous donor or acceptor phases,[15,16] modulate the active layer's electric property by improving the film morphology,[17–19] or tune the acceptor phase optical property,[20] which can promote either the device short-circuit current density (J_{sc}), or open-circuit voltage (V_{oc}), or fill factor (FF), and finally, boost power conversion efficiencies with the values reaching over 13% recently.[21–26]

The ternary approach, by introducing a smaller bandgap nonfullerene acceptor as a near infrared (NIR) absorber to increase the device J_{sc} of fullerene-free binary blended material systems, hereafter named as the "current-increased"

K. Li, M.-A. Pan, Prof. C. Zhan
College of Chemistry and Environmental Science
Inner Mongolia Normal University
Hohhot 010022, China
E-mail: clzhan@iccas.ac.cn

K. Li, M.-A. Pan, Prof. C. Zhan, Prof. J. Yao
CAS Key Laboratory of Photochemistry
Institute of Chemistry
Chinese Academy of Sciences
Beijing 100190, China

The ORCID identification number(s) for the author(s) of this article can be found under https://doi.org/10.1002/aenm.201901728.

K. Li, Dr. Y. Wu, Prof. H. Fu
Beijing Key Laboratory for Optical Materials and Photonic Devices
Department of Chemistry
Capital Normal University
Beijing 100048, China
E-mail: yswu@iccas.ac.cn

Y. Tang, Prof. W. Ma
State Key Laboratory for Mechanical Behavior of Materials
Xi'an Jiaotong University
Xi'an 710049, China
E-mail: msewma@mail.xjtu.edu.cn

DOI: 10.1002/aenm.201901728

strategy, has received an increasing interest recently.[27–33] First, homogeneous acceptor phases can be facilely formed due to their structural similarity between the selected two nonfullerene acceptors.[34,35] Second, the easy structure modifications on the FREA materials benefit the straightforward synthesis of spectrum-complementary acceptor molecules, and the use of the smaller bandgap acceptor as an NIR absorber can produce an increased J_{sc}, and simultaneously, keep the film morphologies[36] with the maintaining of FF.[37] Third, the easy structure modifications again allow scientists to fine-tune the lowest unoccupied molecular orbital (LUMO) and the highest occupied molecular orbital (HOMO) levels of the acceptor molecule. As such, the guest acceptor can be designed with its LUMO level lower than or parallel to the LUMO energy of the host one, thereby a smaller reduction in V_{oc} can be realized in several judiciously designed material systems.[38–40] Based on the judicious design on the ternary material systems, over 13% PCEs have been achieved in this kind of ternary systems.[21]

However, the use of a smaller bandgap nonfullerene acceptor as the NIR absorber cannot increase the device V_{oc}, but usually leads to a decreased V_{oc}, which can even lead to a lower PCE in most cases. In contrast, an even higher V_{oc} would be achieved by introducing a guest acceptor—with its LUMO level lying between the LUMOs of the donor and the host acceptor and again with its HOMO energy lying between the HOMOs of the donor and the host acceptor or parallel to the HOMO of the donor or to the HOMO of the host acceptor—into a binary material system which has deep donor HOMO and gives a high V_{oc} value (**Figure 1**). A big feature of this ternary strategy different to the "current-increased" one is the use of a structurally similar nonfullerene guest acceptor which has a higher LUMO level and blue-shifted spectrum compared to the host one. Though such a "voltage-increased" approach might be universal as the "current-increased" one in designing high-efficiency ternary material systems, it has been, however, still rarely studied for the fullerene-free ternary blended organic solar cells in which both the acceptor components are nonfullerene molecules. The big challenge is the difficulty to find such a nonfullerene guest acceptor which not only has a higher LUMO level and a proper deep HOMO level so as to optimize the acceptor-phase energy levels to the ideal form as mentioned above (Figure 1) but also forms homogeneous acceptor phases with the maintaining or even improving of film morphology so that the large J_{sc} and FF can be maintained or even increased.

So far there have been reported only several ternary cases featuring with the "voltage-increased" approach. Three of them showed simultaneous boosting of V_{oc}, J_{sc}, and FF. The PCEs of the ternary system, PSTZ:ITIC:IDIC (1:0.1:0.9), J71:IT-M:ITIC (1:0.9:0.1), PBDB-T:IT-CN:IT-4M (1:0.2:0.8), and PM6:MeIC:ITCPTC (1:0.6:0.4), respectively, reach 11.1% with improvement of the acceptor phase crystallinity,[41] 11.60% (4% sacrifice of FF),[42] 12.2%,[43] and 14.13% by replacing 60% of ITCPTC with the greater crystalline MeIC.[44]

In this work, we select PM6:IT-4F and PM6:Y6 (**Figure 2**a), the two high-efficiency binary material systems, which exhibit a high V_{oc} of 0.83 and 0.85 V, respectively, as the host systems. We choose IDIC (Figure 2a) as the guest nonfullerene acceptor to obtain an even increased V_{oc} because IDIC has a higher LUMO level than the host IT-4F and Y6 and its structure is similar to the host acceptor. The two ternary systems obtained by adding IDIC into the PM6:IT-4F and PM6:Y6 blend demonstrate a broad tolerance of the device function on the acceptor proportions with the PM6:IDIC:IT-4F(Y6) ratio ranging from 1:0:1 to 1:0.7:1 and over 11.8% and 12.9% efficiencies can be obtained even as the IDIC content reaches 0.7 in which the total donor:acceptor ratio reaches 1:1.7. The champion devices are obtained with the mixing of 0.2 IDIC. An impressive efficiency of 16.5% is obtained from the best device with Y6 as the electron acceptor. For the IT-4F best device, the best PCE is 14.0%. The PCEs of the PM6:Y6 and PM6:IT-4F devices are 15.4% and 12.9%, respectively. In comparisons to the binary devices, V_{oc} and FF are simultaneously increased, and at the same time, a small increase in J_{sc} is observed. After the addition of 0.2 IDIC, the homogeneous fine film morphology and the π–π stacking patterns of the host donor:acceptor blend are well kept, and meanwhile, larger donor and acceptor phases are formed. The increased charge mobilities and the reduced recombination allow us to obtain the best ternary devices with a relatively thicker active layer (110 vs 100 nm), which plus the absorption from the added IDIC account for the small increase of J_{sc}. The reduced trap-assisted Shockley–Read–Hall (SRH) and the geminate recombination are the reasons for the improved device FF for the IT-4F system, and for the Y6 system, the increased charge mobilities and the reduced trap-assisted Shockley–Read–Hall are likely the reasons.

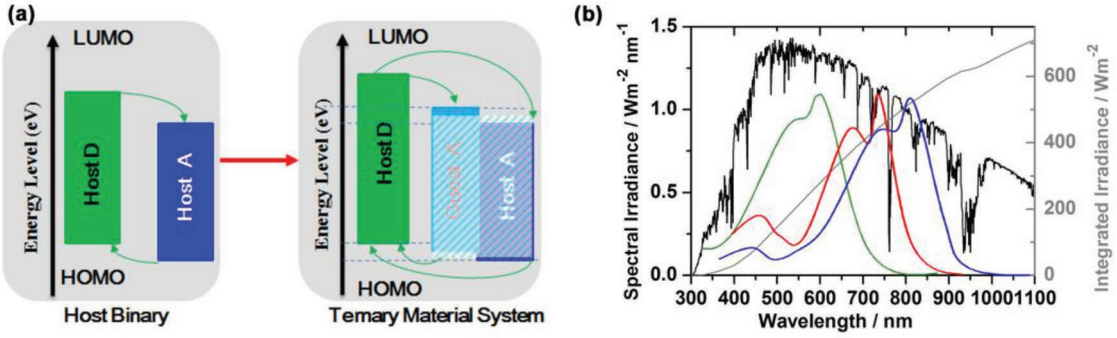

Figure 1. a) Energy alignments and b) spectral features of the ternary material system featuring increased V_{oc} in comparison to the host binary.

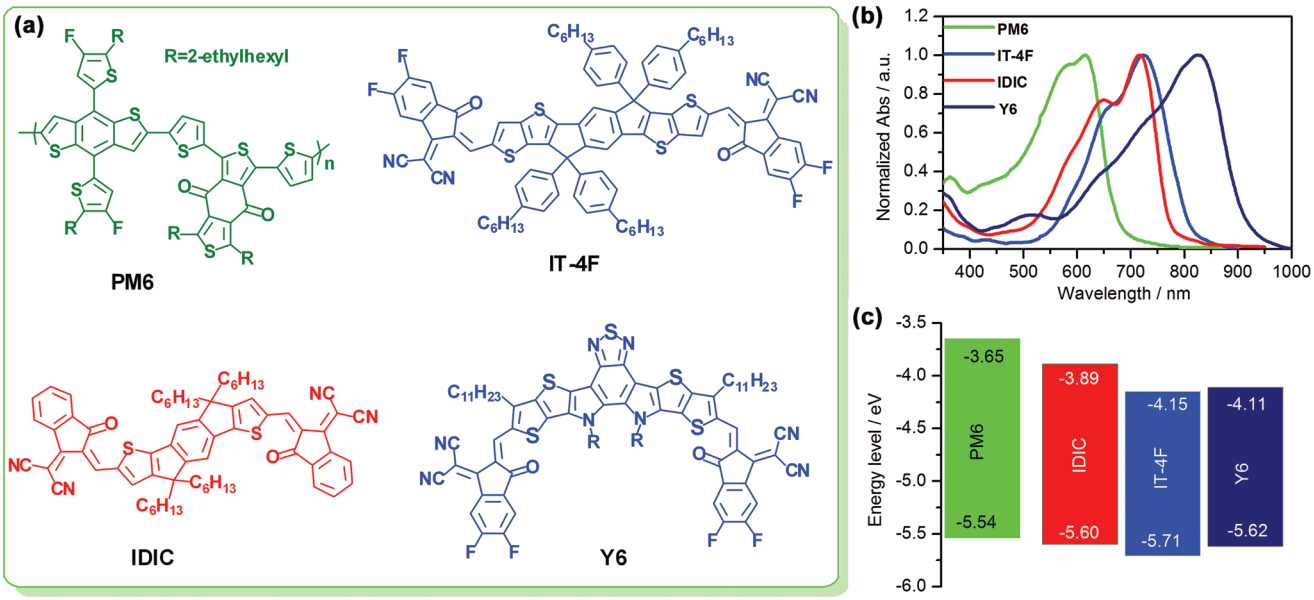

Figure 2. a) Chemical structures of the donor polymer PM6[45] and the structurally similar FREAs, IT-4F[46] or Y6[13] and IDIC,[47] used in this work. b,c) Film absorption spectra and energy levels of PM6, IDIC, IT-4F, and Y6. The energy levels of the materials are all measured under the same conditions.

2. Results

2.1. Optical and Electrochemical Properties

The neat film absorption spectra of the donor polymer and nonfullerene acceptors are shown in Figure 2b. The absorption of PM6 ranges from 400 to 700 nm with two peaks at 580 and 612 nm. The absorption peaks are at 664 and 721 nm for IT-4F and at 648 and 720 nm for IDIC. The full-width-at-the-half-maximum (FWHM) values of the IT-4F and IDIC film absorption are nearly identical. The absorption of PM6 complements the absorption of IT-4F and IDIC very well. The absorption onset occurs at 828 and 782 nm, corresponding to an E_g^{opt} of 1.50 and 1.59 eV, respectively, for IT-4F and IDIC. Compared to IT-4F, Y6 shows an even broader absorption with the absorption peak red-shifting to 828 nm and the onset appearing at 935 nm which corresponds to a much smaller E_g^{opt}, 1.33 eV. Relatively to IT-4F, the Y6 ternary more fully covers the near infrared solar emission spectrum with its absorption more complementary to the IDIC and PM6 absorption.

Figure 2c shows the energy level diagrams of the four materials. The energy levels were tested by cyclic voltammetry under the same experimental conditions (Figure S1, Supporting Information). The HOMO/LUMO levels are −5.50/−3.69 eV for PM6, −5.60/−3.89 eV for IDIC, −5.71/−4.15 eV for IT-4F, and −5.62/−4.11 eV for Y6, respectively. The LUMO of IDIC positions between the LUMO of PM6 and the LUMO of IT-4F/Y6 with its energy level higher than the LUMO level of IT-4F/Y6 by more than 0.2 eV (Figure 2c). In energy level, the HOMO of IDIC is higher than the HOMO of IT-4F and parallel to the HOMO level of Y6, but it is lower than the HOMO of PM6 by 0.06 eV, which means IDIC can be used as the electron acceptor material in these two ternary systems.

2.2. Photovoltaic Property

The photovoltaic properties by using IDIC as the guest acceptor component were first tested by introducing IDIC into the PM6:IT-4F binary system and the binary and ternary solar cells were fabricated using the traditional structure with ITO (indium tin oxide)/PEDOT:PSS/active layer/PDINO/Al. Here, PEDOT:PSS is poly(3,4-ethylenedioxythiophene):poly(styrene sulfonate) and PDINO is *N*,*N*-bis(3,3-dimethyl-3-amino *N*-oxide-*n*-propyl)perylene diimide. The weight ratios of PM6:IT-4F in the binary and ternary active layers were fixed as 1:1, while the ratio of IDIC was changed as PM6:IDIC:IT-4F = 1:*x*:1; here *x* is the ratio of IDIC (**Table 1**). 0.5% of 1,8-diiodooctane (DIO) (Table S1, Supporting Information) was added and the as-cast blend film was annealed at 90 °C for 10 min. For the ternary blended systems of PM6:IDIC:IT-4F = 1:*x*:1, the champion devices were obtained as $x = 0.2$. The optimizations are given in Tables S2–S4 in the Supporting Information. The active layer thickness was ≈100 nm for the binary blend, and ≈110 nm for the 1:0.2:1 ternary blend (Table S5, Supporting Information).

The current density–voltage (*J*–*V*) curves of the optimal binary and ternary solar cells are shown in **Figure 3**a. The binary cell has a V_{oc} of 0.833 V, a J_{sc} of 20.60 mA cm^{-2}, an FF of 75.04%, and a PCE of 12.88%. The average PCE is 12.64% (Table 1). IDIC is poorly soluble in chlorobenzene (CB) and then 10 mg mL^{-1} CB solution, rather than 20 mg mL^{-1}, of PM6:IDIC was used to prepare the PM6:IDIC active layer. The PM6:IDIC solar cell with an active layer thickness of ≈70 nm has a PCE of 7.13% with V_{oc} = 0.924 V, J_{sc} = 10.81 mA cm^{-2}, and FF = 71.6%, respectively. Compared to the PM6:IDIC binary, the IT-4F binary shows excellent film-forming property. For the ternary blend with PM6:IDIC:IT-4F = 1:*x*:1, the good film-forming property can be maintained well even as the IDIC

Table 1. Summary of the photovoltaic data of the IT-4F and Y6 based optimal binary and ternary devices with the variations of the IDIC contents. All the data were obtained under illumination of AM 1.5G, 100 mW cm^{-2} light source.

PM6:IDIC:host = 1:*x*:1		V_{oc}[a)] [V]	J_{sc}[a)] [mA cm^{-2}]	FF[a)] [%]	PCE[a)] [%]
IT-4F	$x = 0$	0.833 (0.832 ± 0.002)	20.60 (20.37 ± 0.22)	75.04 (74.50 ± 0.52)	12.88 (12.64 ± 0.20)
	$x = 0.1$	0.842 (0.841 ± 0.001)	20.65 (20.48 ± 0.19)	76.17 (75.70 ± 0.44)	13.24 (13.09 ± 0.12)
	$x = 0.2$	0.869 (0.869 ± 0.001)	20.98 (20.74 ± 0.22)	77.00 (76.20 ± 0.78)	14.03 (13.79 ± 0.22)
	$x = 0.3$	0.881 (0.879 ± 0.002)	20.73 (20.20 ± 0.40)	75.58 (74.16 ± 1.40)	13.80 (13.63 ± 0.14)
	$x = 0.4$	0.862 (0.859 ± 0.003)	20.75 (20.23 ± 0.50)	74.11 (73.17 ± 0.90)	13.26 (12.96 ± 0.27)
	$x = 0.5$	0.861 (0.860 ± 0.001)	20.52 (20.28 ± 0.21)	72.87 (71.61 ± 1.23)	12.87 (12.66 ± 0.18)
	$x = 0.6$	0.862 (0.861 ± 0.001)	19.80 (19.67 ± 0.11)	72.49 (70.96 ± 1.49)	12.37 (12.24 ± 0.11)
	$x = 0.7$	0.864 (0.863 ± 0.001)	18.71 (18.52 ± 0.16)	72.47 (70.34 ± 1.10)	11.67 (11.39 ± 0.24)
Y6	$x = 0$	0.857 (0.854 ± 0.003)	25.05 (24.87 ± 0.15)	71.95 (71.62 ± 0.30)	15.45 (15.20 ± 0.23)
	$x = 0.1$	0.862 (0.861 ± 0.001)	25.12 (24.98 ± 0.12)	73.37 (73.02 ± 0.21)	15.88 (15.72 ± 0.13)
	$x = 0.2$	0.868 (0.867 ± 0.001)	25.39 (25.23 ± 0.13)	74.92 (74.50 ± 0.40)	16.51 (16.28 ± 0.20)
	$x = 0.3$	0.877 (0.875 ± 0.002)	25.02 (24.72 ± 0.27)	72.51 (72.04 ± 0.43)	15.90 (15.73 ± 0.14)
	$x = 0.4$	0.886 (0.885 ± 0.001)	24.84 (24.55 ± 0.26)	69.99 (69.71 ± 0.25)	15.39 (15.20 ± 0.16)
	$x = 0.5$	0.885 (0.884 ± 0.001)	24.78 (24.32 ± 0.44)	69.04 (68.71 ± 0.30)	15.14 (15.00 ± 0.12)
	$x = 0.6$	0.881 (0.870 ± 0.001)	24.44 (24.13 ± 0.30)	68.54 (68.12 ± 0.40)	14.75 (14.52 ± 0.20)
	$x = 0.7$	0.881 (0.880 ± 0.002)	21.62 (21.17 ± 0.42)	67.91 (67.56 ± 0.32)	12.93 (12.70 ± 0.21)

[a)]The average values were obtained from 20 devices.

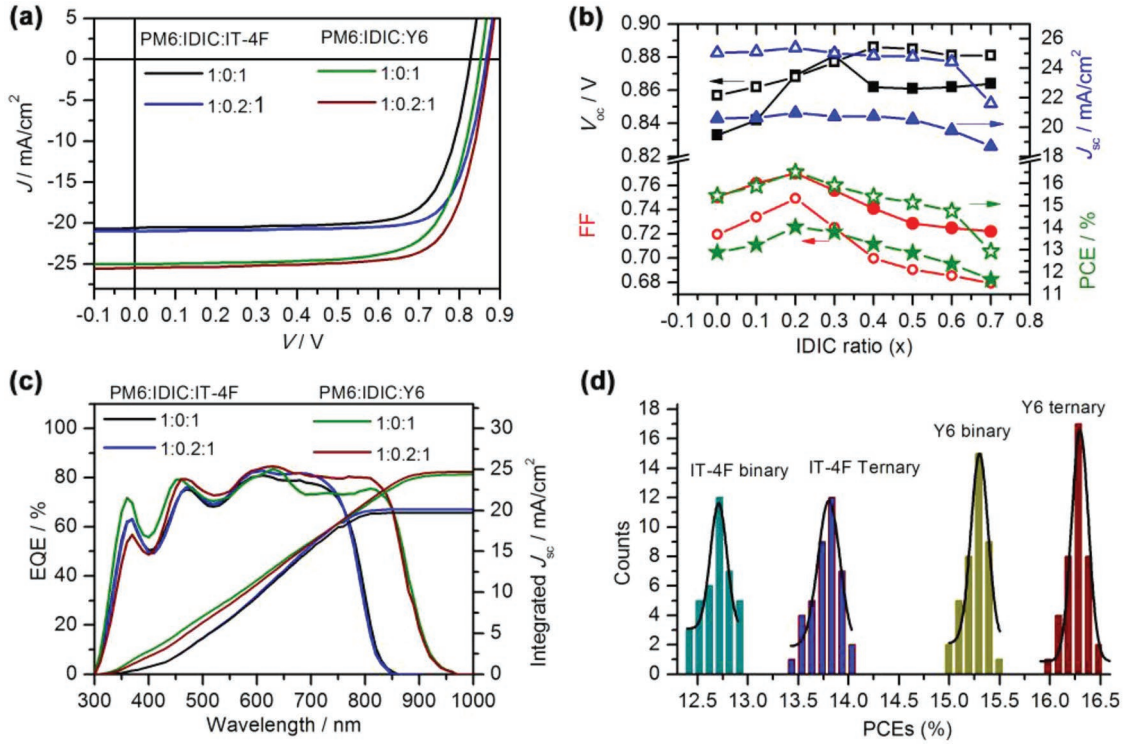

Figure 3. a) The *J*–*V* curves of the optimal binary (PM6:IT-4F = 1:1 and PM6:Y6 = 1:1) and ternary (PM6:IDIC:IT-4F = 1:0.2:1 and PM6:IDIC:Y6 = 1:0.2:1) solar cells. b) The changes of V_{oc}, FF, J_{sc}, and PCE with the variations of the IDIC composites for the IT-4F (filled symbols) and Y6 (hollow symbols) based ternary devices. c) The EQE spectra and integrated J_{sc} of the optimal binary and the 1:0.2:1 based ternary solar cells. d) The efficiencies histograms of the IT-4F and Y6 based binary and ternary blends.

ratio is up to 0.7 and a PCE of 11.7% is yet obtained (Table 1) though its J_{sc} and FF became lower than that of the PM6:IT-4F binary device. The good device performance obtained with the IDIC content of x from 0.1 to 0.7 suggests that the PM6:IT-4F binary blend is of broad tolerance of the addition of the poor film-forming IDIC (Figure 3b). As the IDIC content is more than 0.8, particle aggregates can be visible to the naked eye and the device performance deteriorates significantly. The best performance is obtained at $x = 0.2$ and a PCE of 14.03% is obtained with an increased V_{oc} of 0.869 V, a higher FF of 77.00%, and also an increased J_{sc} of 20.98 mA cm^{-2}. Figure 3c shows the external quantum efficiency (EQE) spectra of the optimal binary and ternary devices. Their integrated short-circuit currents are 19.69 and 20.12 mA cm^{-2}, respectively, which are consistent with the J_{sc} values tested from the J–V measurements.

For the Y6 binary, a PCE of 15.45% with $V_{oc} = 0.857$ V, $J_{sc} = 25.05$ mA cm^{-2}, and FF = 71.95% is obtained. The J–V curve is given in Figure 3a. A wide tolerance of the IDIC compositions is also observed with the PM6:IDIC:Y6 ratios going from 1:0:1 to 1:0.7:1 and a PCE of 12.9% is still obtained as $x = 0.7$ (Figure 3b and Table 1). The best performance is observed as 0.2 IDIC is used, which supplies a PCE of 16.51%. An increased V_{oc} (0.857 vs 0.868 V), an increased FF (71.95% vs 74.92%), and an increased J_{sc} (25.05 vs 25.39 mA cm^{-2}) are obtained. We sent the best device to the National Institute of Metrology (NIM), China and received a certificated efficiency of 15.4% (Figure S2, Supporting Information). The ternary device with a film thickness of 294 nm still shows a PCE of 11.7% (Table S4, Supporting Information). Figure 3d gives the histograms of the PCEs for the PM6:IT-4F and PM6:Y6 based binary devices and their ternary devices with the addition of 0.2 IDIC. Figure 3c gives the EQE of the best binary and ternary devices. The integrated J_{sc} values are 24.34 and 24.67 mA cm^{-2} for the binary and ternary solar cells, respectively, which well agree with the J_{sc} values obtained from the J–V measurements.

2.3. Charge Mobilities, Recombination, and Collection

The hole and electron mobilities (μ_h/μ_e) were measured with space charge limited current (SCLC) method (Figure S3, Supporting Information) with the structures of ITO/PEDOT:PSS/active layer/Au (hole only) and ITO/TIPD/active layer/PDINO/Al (electron only), respectively. The μ_h/μ_e values (**Figure 4**a) are $4.80/4.60 \times 10^{-4}$, $6.85/6.52 \times 10^{-4}$, and $3.32/8.62 \times 10^{-4}$ cm^2 V^{-1} s^{-1} for the IT-4F, IDIC, and Y6 binary blends, respectively. The IDIC binary exhibits a little larger hole and electron mobilities than the IT-4F blend, while the Y6 blend has even larger electron mobility, but shows a smaller hole mobility. With the introduction of IDIC as the guest acceptor component, the μ_h/μ_e values increase to $6.10/5.55 \times 10^{-4}$ cm^2 V^{-1} s^{-1} for the IT-4F ternary and $6.02/12.6 \times 10^{-4}$ cm^2 V^{-1} s^{-1} for the Y6 ternary.

To investigate the effect of the insertion of IDIC on the charge collection and recombination mechanisms, we first measured the light dependent J–V characteristics, from which the relationships between V_{oc}/J_{sc} and light intensity (P)[48] were plotted and shown in Figure 4b,c. The recombination at open circuit can be reflected by the plot of the open-circuit voltage as a function of the light intensity (P) by following Eq. $V_{oc} \propto n(KT/q)\ln(P)$, where k, T, and q are the Boltzmann constant, temperature in Kelvin, and the elementary charge, respectively.

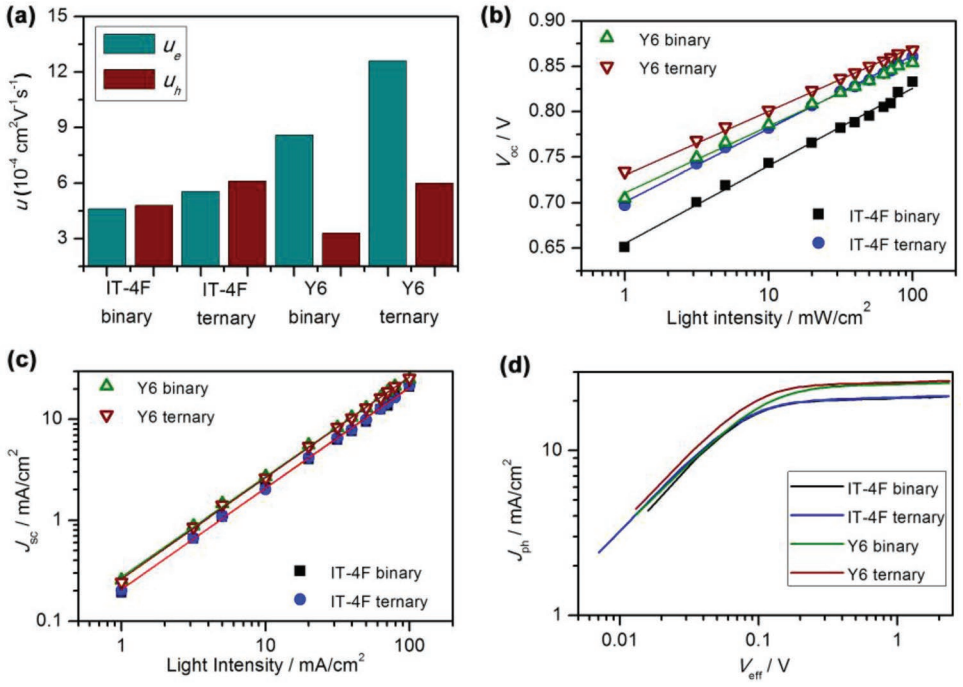

Figure 4. a) Distributions of the hole and electron mobilities of the IT-4F and Y6 based binary and ternary blended solar cell films. Plots of V_{oc} b) and J_{sc} c) versus incident light intensity and J_{ph} versus V_{eff} characteristics d) of the IT-4F and Y6 based optimal binary and ternary devices.

The fitting n values are 1.42 KT/q and 1.31 KT/q for the IT-4F binary and ternary and 1.22 KT/q and 1.16 KT/q for the Y6 binary and ternary devices, respectively. The smaller n value suggests reduced trap-assisted Shockley–Read–Hall or the geminate recombination, which says that 1) for both the IT-4F and Y6 systems, the mixing of 0.2 IDIC can reduce the SRH or geminate recombination and 2) compared to the IT-4F systems, the Y6 devices show reduced trap-assisted SRH or the geminate recombination. The recombination at the short-circuit condition can be suggested by the plot of J_{sc} as a function of light intensity in a power law equation $J_{sc} \propto P^{\alpha}$. The fitting α values are 0.984 and 0.995 for the PM6:IT-4F binary and ternary and 0.991 and 0.997 for the Y6 binary and ternary devices, respectively. The fitting α value for the ternary device is closer to 1, suggesting that the bimolecular recombination might be reduced slightly with the addition of 0.2 IDIC. Taken together, reduced recombination is observed upon the addition of 0.2 IDIC into the 1:1 blended PM6:IT-4F and PM6:Y6 systems.

We again measured the photocurrent (J_{ph}) as a function of the effective voltage (V_{eff}) (Figure 4d),[49] with $V_{eff} = V_{BI} - V_{bias}$, where V_{BI} is the voltage when $J_{ph} = 0$ mA cm^{-2}, and V_{bias} is the applied voltage, and $J_{ph} = J_D - J_L$, where J_L and J_D are the current densities under illumination and dark conditions, respectively. As shown, at the large applied voltage regime ($V_{eff} > 2.0$ V), J_{ph} becomes saturated, indicating that almost all photogenerated excitons are dissociated and the generated free charge carriers are collected by the electrodes. The charge collection efficiency was calculated to be 96.3%, 98.7%, 96.1%, and 97.3% for the IT-4F binary, IT-4F ternary, Y6 binary, and Y6 ternary, respectively. The addition of 0.2 IDIC to form a ternary blend improves the charge collection efficiency for both the IT-4F and Y6 systems.

2.4. Transient Absorption Spectroscopy

Femtosecond transient absorption spectroscopy (fs-TA) technique was carried out on the blended films to investigate the effects of the addition of IDIC on the hole transfer process and recombination dynamics by selective excitation of the nonfullerene acceptor, i.e., IT-4F or Y6 in the binary, and IT-4F:IDIC or Y6:IDIC in the ternary. For the IT-4F systems, the TA spectra were monitored upon excitation at 760 nm, at which wavelength only the acceptor materials are selectively excited (Figure 1c) and not any TA signals can be observed for PM6-only film. As shown in **Figure 5**a, ground state bleaching (GSB) band at 730 nm, which is caused by IT-4F/IDIC, can be observed at 0.12 ps after excitation. Almost simultaneously, the GSB band correlated with PM6 at 635 nm also appears. Since energy transfer from IDIC/IT-4F to PM6 is inaccessible considering the lower singlet energies of the acceptors relative to that of PM6, the promptly emerging PM6 GSB can only be caused by the hole transfer from IDIC/IT-4F to PM6 and the charge carrier indicated by the 635 nm GSB signal is generated within the time resolution of our apparatus (with a rate <200 fs). Figure 5b compares the charge recombination process shown as the kinetic curves at 635 nm for PM6:IT-4F and PM6:IDIC:IT-4F blends. The decay of the 635 nm GSB signal for PM6:IT-4F film can be well fitted with a two-exponential function, resulting in two lifetimes of 0.56 and 330 ps, respectively. This decay process is slowed down in PM6:IDIC:IT-4F (1:0.2:1) blend, producing two lifetimes of 4.0 ps and 2.3 ns. In one word, for the IT-4F system, both the binary and ternary blends undergo a very fast hole transfer and a prolonged charge separated state produced via the hole transfer is observed in the ternary blend.

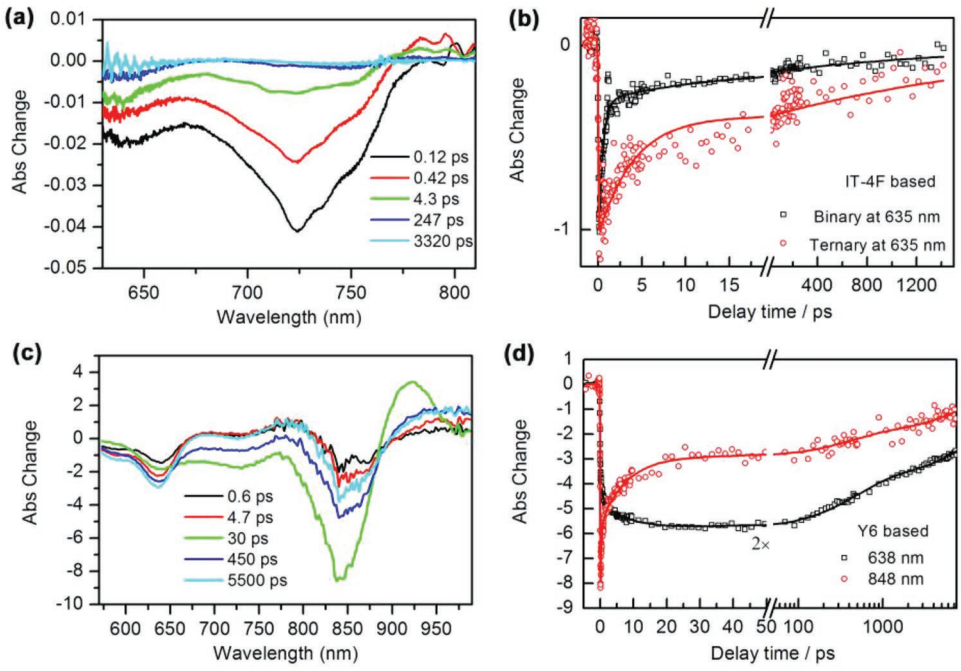

Figure 5. a) TA data for ternary system of PM6:IDIC:IT-4F (1:0.2:1) blend film upon excitation at 760 nm. b) Comparisons of the 635 nm kinetic curves for PM6:IT-4F (1:1) and PM6:IDIC:IT-4F (1:0.2:1) blend films. c) TA data for ternary system of PM6:IDIC:Y6 (1:0.2:1) blend film upon excitation at 840 nm. d) Comparisons of the kinetic curves of the 638 and 848 nm GSB signals for PM6:IDIC:Y6 (1:0.2:1) film.

Compared to IT-4F, Y6 exhibits a much red-shifted absorption spectrum. This allows us to be possible to selectively excite Y6 or Y6:IDIC and to see the effects of the added IDIC on the generation of the PM6 GSB signal via the hole transfer process. The 840 nm light was used to monitor the exciton dynamics for the blends of Y6 series, which selectively excited the Y6. After excitation, a clear GSB signal at 848 nm and excited state absorption (ESA) band over 900 nm appear in both neat Y6 (Figure S4, Supporting Information) and the blends (Figure 5c; Figure S5, Supporting Information). As time proceeds, a new negative band at 638 nm gradually builds up for PM6:IDIC:Y6 blend (Figure 5c), which can be assigned to the GSB of PM6. Since energy transfer from Y6 to PM6 is inaccessible considering the lower singlet energies of Y6 relative to that of PM6 and IDIC, the increment of GSB intensity of PM6 is mostly caused by the hole transfer from Y6 or Y6:IDIC to PM6. The hole transfer rate can be calculated from the analysis of the initial stage of 638 nm kinetic curve, producing a rising lifetime of 3.9 ps. Both the Y6 848 nm and PM6 638 nm GSB bands decay in concert with a time constant of 6.6 ns (Figure 5d), which is much slower than the intrinsic lifetime of pristine Y6 film (129 ps; Figure S4b, Supporting Information). No appreciable spectral difference can be observed for PM6:Y6 film compared with PM6:IDIC:Y6 film (Figure S5, Supporting Information). When the pump wavelength was set to 760 nm, both IDIC and Y6 were excited in PM6:IDIC:IT4F blend (Figure S6a, Supporting Information). In addition to the typical spectral signatures of Y6 GSB (850 nm), PM6 GSB (638 nm), and S_1 absorption of Y6 (910 nm), the IDIC GSB is shown as a small dip at around 740 nm (Figure S6a, Supporting Information). Due to severe overlapping caused by Y6 GSB, the evolution of IDIC GSB band cannot be traced separately. The increment of 638 nm GSB signal speeds up from 3.9 (excited using the 840 nm light) to 0.79 ps for PM6:Y6 system as a result of hot exciton generation and dissociation.[50,51] As for PM6:IDIC:Y6, this process was further accelerated, with two rising time constants of 0.15 and 0.82 ps, respectively (Figures 5d; Figure S6b, Supporting Information). The 0.8 ps component can be assigned to be the hole transfer from Y6 to PM6, whereas the 0.15 ps component is due to the hole transfer from IDIC to PM6. That indicates the introduction of IDIC opens an additional rapid hole transfer channel and contributes to the carrier generation in the ternary system.

2.5. Film Morphology

To see the changes of phase crystallinity and molecular packing of the nonfullerene acceptor IT-4F/Y6 and the donor polymer PM6 after IDIC is blended with them, we conducted the graze-incidence wide-angle X-ray scattering (GIWAXS) experiments and **Figure 6** shows the GIWAXS data of the binary and the ternary blends. For the Y6 blends, the donor and nonfullerene acceptor perform perfect face-on orientation as suggested by the (010) signal appearing mainly at the q_z direction (around 1.75 $Å^{-1}$) and the lamellar (100) signal seen at the q_{xy} direction (around 0.29 $Å^{-1}$). The additional peak at 0.425 $Å^{-1}$ ($d \approx 14.8$ Å) in the in-plane direction could be originated from the backbone ordering previously found in Y6 film.[13,52] The scattering patterns of the PM6 and Y6 are well kept and the coherent crystalline length (CCL) of the π–π stacking (4.59 vs 4.77 nm) is maintained after the addition of 0.2 IDIC. For the PM6:IT-4F system, the face-on oriented π–π stacking signal appears around 1.78 $Å^{-1}$ ($d \approx 3.53$ Å). The peak around 1.35 $Å^{-1}$ ($d \approx 0.46$ Å) could be due to the packing ordering of the perpendicular side chains of IT-4F, as observed previously by us from the ITCT-DM molecule.[53] Upon the mixing with 0.2 IDIC, the π–π stacking scattering signal is seen around 1.77 $Å^{-1}$ ($d \approx 3.55$ Å), featuring the addition of the (010) signals of the IT4F binary and the IDIC binary. The CCL reflecting the crystalline size of the π–π stacking is estimated to be 3.86 nm for both the IT-4F binary blend and its ternary blend with the addition of 0.2 IDIC. The packing ordering of PM6 in the IT-4F system can be analyzed from the out-of-plane (OOP) lamellar signal

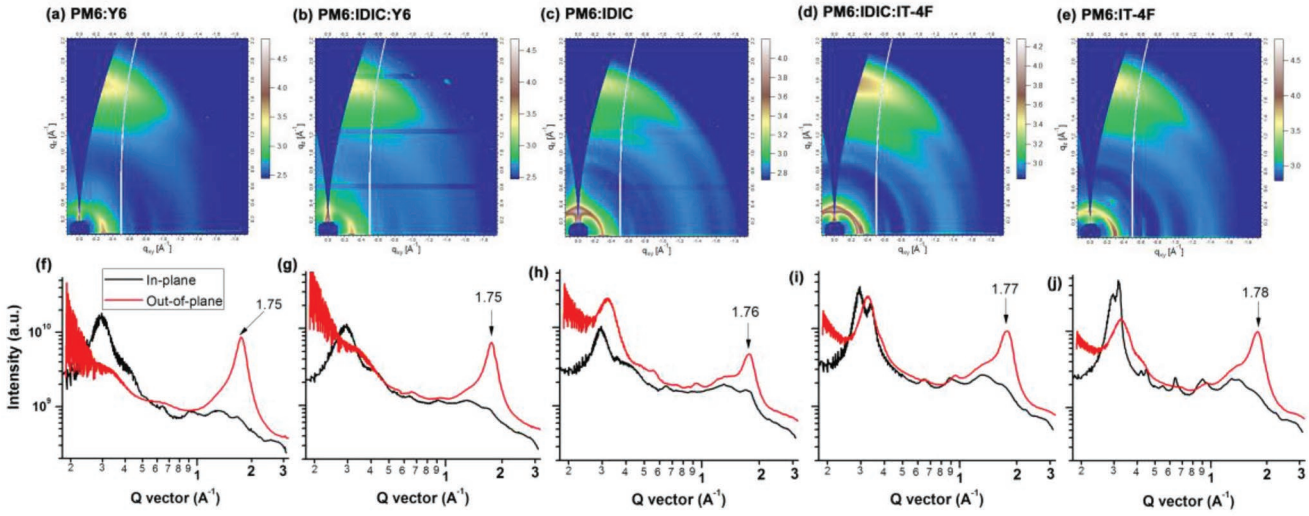

Figure 6. a–e) The 2D GIWAXS pictures and f–j) the line cut profiles of the PM6:Y6 (1:1, a and f), PM6:IDIC:Y6 (1:0.2:1, b and g), PM6:IDIC (1:1, c and h), PM6:IDIC:IT-4F (1:0.2:1, d and i), and PM6:IT-4F (1:1, e and j), respectively.

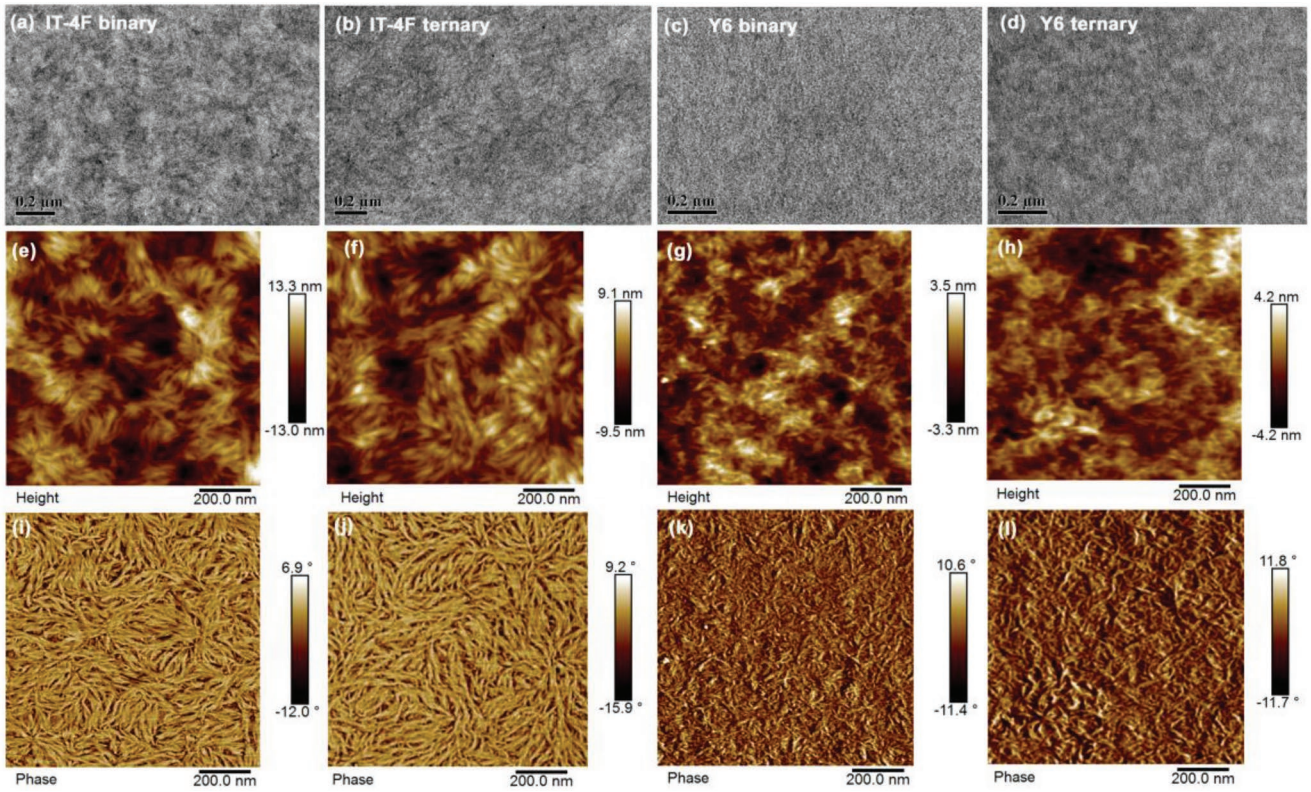

Figure 7. a–d) Magnified TEM and e–h) 1 μm × 1 μm scaled AFM height and i–l) phase images of the IT-4F binary (PM6:IT-4F = 1:1, a, e, and i), IT-4F ternary (PM6:IDIC:IT-4F = 1:0.2:1, b, f, and j), Y6 binary (PM6:Y6 = 1:1, c, g, and k), and Y6 ternary (PM6:IDIC:Y6 = 1:0.2:1, d, h, and l), respectively.

around 0.32 $Å^{-1}$ ($d \approx 9.82$ Å) with the CCL increasing from the binary 14.3 nm to the ternary 18.5 nm. The scattering intensity of the OOP 0.32 $Å^{-1}$ signal becomes intense after the addition of 0.2 IDIC. For the Y6 system, the lamellar signal seen at the OOP direction is very weak, appearing as a very broad band around 0.34 $Å^{-1}$. Its intensity becomes a little intense after the addition of 0.2 IDIC, which implies the small increase of the lamellar crystallinity.

The film morphologies of the binary and ternary blended solar cell films are again characterized with transmission electron microscopy (TEM) and atomic force microscopy (AFM) and their images are shown in **Figure 7**. For the IT-4F and Y6 based blends, nanoscaled and separated fine white and dark phases are clearly seen either on their binary or their ternary blends, which are consistent well with their high device performance. Fine differences can be seen on their AFM images. In the AFM height and phase images, the bright and brown phases can be assigned to the donor- and acceptor-rich domains, respectively. Longer and larger white phases are seen after the addition of 0.2 IDIC into the 1:1 blended PM6:IT-4F or PM6:Y6, which is consistent with the more intense intensity of the lamellar 0.32/0.34 $Å^{-1}$ scattering signal and the increased hole mobilities. With the formation of the larger and longer donor-rich fibrils, larger fibril-like acceptor-rich domains can be seen on the ternary TEM and AFM pictures, which is in agreement with the increased electron mobilities. Compared to the longer and larger white fibers seen on the IT-4F based blends, finer and shorter fibers are seen on the Y6-based blends, either for the binary or the ternary. The shortest white fibers observed in the Y6 binary are in concert with the weakest scattering intensity of the lamellar 0.34 $Å^{-1}$ signal and its smallest hole mobility. The root-mean-square (RMS) roughness is 3.71 nm for the IT-4F binary, which is decreased slightly to 2.84 nm for the IT-4F ternary. Much smooth surface is seen for the Y6 binary and its ternary blends with a RMS roughness of 0.94 and 1.25 nm, respectively.

3. Discussion

The solar cell data (Table 1) clearly demonstrate the effectiveness of the use of IDIC as the extra acceptor component to increase the device efficiencies of the PM6:IT-4F and PM6:Y6 binary material systems. In both systems, the V_{oc}, FF, and J_{sc} are simultaneously increased. The homogeneous fine film morphologies and the π–π stacking patterns of the host binary blend, PM6:IT-4F or PM6:Y6, are well maintained after the addition of 0.2 IDIC, which could be the morphological basis of the effectiveness of this ternary approach. Moreover, improvement of the film morphology is also observed, as suggested by the formation of larger and longer fibril donor-rich phases and the formation of larger fibril-like acceptor-rich domains and also by the observation of the increased crystallinity of the lamellar packing indicated by the OOP 0.32/0.34 $Å^{-1}$ signal.

The LUMO level of IDIC is higher than the LUMO energy of Y6/IT-4F by 0.22/0.26 eV, and its HOMO level is higher than

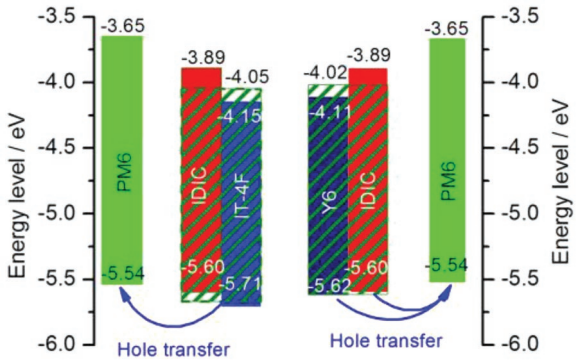

Figure 8. Diagram of the energy levels of the donor, individual acceptor, and the mixed acceptors, and possible kinetic models of the hole transfer in the IT-4F and Y6 systems.

that of Y6/IT-4F by 0.02/0.11 eV. Blending of IDIC with Y6/IT-4F shifts the LUMO to −4.02/−4.05 eV for the Y6:IDIC and IT-4F:IDIC blends (1:0.2) (**Figure 8**), as calculated from the CV data of the blended films (Figure S7, Supporting Information). The HOMO energy is shifted to −5.67 eV for the IT-4F:IDIC blend and for the Y6:IDIC blend no upshifts are detected. The upshifted LUMO levels of Y6:IDIC and IT-4F:IDIC blend account for the increased V_{oc} of the ternary devices compared to their binary counterparts.

As seen from Figure 3a, the reduced recombination at the open-circuit condition mainly accounts for the improved device FF. This is further supported by the results from the light dependent *J*–*V* measurements as shown in Figure 4b,c, in which a large decrease is seen from the *n* values, while the α values are observed between 0.98 and 1.00. A relatively larger decrease with the *n* value from the binary 1.42 *KT/q* to the ternary 1.31 *KT/q* is seen for the IT-4F system, and for the Y6 system, the *n* value is slightly decreased from the binary 1.22 *KT/q* to the ternary 1.16 *KT/q*. The decrease of the *n* value indicates the reduction of the monomolecular recombination, either from the trap-assisted SRH or the geminate. The studies on the hole transfer process (Figure 5) indicate that for the IT-4F system, the very fast hole transfer with a rate <200 fs observed in both the binary and ternary blends and the prolonged charge separated state with lifetimes of 4.0 ps and 2.3 ns produced in the ternary blend via the hole transfer process may contribute to a reduction of geminate recombination. On the basis of these results, the increased device FF for the IT-4F ternary is most likely to contribute to the reduction of the trap-assisted SRH and the geminate recombination. For the Y6 system, the fast hole transfer with a rate of 3.9 ps and the slow decay with a rate of 6.6 ns also contribute to reduce the geminate recombination in both the binary and ternary blends and the added 0.2 IDIC acts as a fast additional hole transfer channel to that of the host Y6 to produce charge carriers (Figure 8). Based on the results on hand, the increase of the device FF with the addition of 0.2 IDIC is likely due to the reduction of trap-assisted SRH recombination and the large increase of the charge carrier mobilities with the hole–electron mobilities becoming more balanced (0.478 vs 0.385).

The increased charge mobilities and the reduced recombination allow us to obtain the champion ternary device in a relatively thicker ternary blended active layer, that is, 110 nm compared to the 100 nm thickness of the binary blended active layer. Again, we fabricated the ternary blended active layer in a weight ratio of PM6:IDIC:Y6(IT-4F) of 1:0.2:1. The absorption of the solar photons by the host donor:acceptor blend, PM6:Y6 and PM6:IT-4F, could be close to each other in the ternary blend and in the binary blend, while the added IDIC contributes to additional absorption, as suggested by the absorption spectra of the blended absorption spectra (Figure S8, Supporting Information). For the IT-4F and Y6 system, the increased J_{sc} can be due to the contribution of the added IDIC to EQE as suggested by the EQE increase in the wavelength region of 630–760 nm, in the region of the absorption of IDIC. For the Y6 system, the contribution is again indicated by the increased EQE in the 460–630 and 750–850 nm regions, which can be due to the contributions from the increased hole and electron mobilities.

4. Conclusions

In summary, we report herein a highly efficient ternary blended fullerene-free polymer solar cell with an efficiency of 16.5%, which is achieved with a simple yet effective ternary approach by using IDIC as the guest acceptor component of the binary system of PM6:Y6. The effectiveness of this approach is demonstrated with the same beneficial effects of the simultaneous increases in V_{oc}, FF, and J_{sc} in another material system of PM6:IT-4F. The higher LUMO level of IDIC than Y6 and IT-4F is one reason of the increased V_{oc}. The reduced trap-assisted RSH and the geminate recombination as suggested from the light-dependent *J*–*V* measurements and the study on the hole transfer are the reasons for the increased FF for the IT-4F system. For the Y6 system, the increased FF may be due to the reduction of trap-assisted SRH recombination and the large increase of the charge carrier mobilities. The increased J_{sc} is contributed from the absorption from the added IDIC and the relatively thicker active layer (110 vs 100 nm), and for the Y6 system, it is also contributed from the increased charge mobilities. For the Y6 system, the added IDIC acts as a fast additional hole transfer channel to contribute to the carrier generation.

Supporting Information

Supporting Information is available from the Wiley Online Library or from the author.

Acknowledgements

The authors gratefully acknowledge the financial support of the National Natural Science Foundation of China (NSFC, Grant Nos. 91433202, 21327805, 21773262, 21833005, 21504066, 21534003, and 91227112), the Chinese Academy of Sciences (CAS, XDB12010200), and the Ministry of Science and technology (Grant No. 2016YFA0200700). X-ray data were acquired at beamlines 7.3.3 at the Advanced Light Source, which is supported by the Director, Office of Science, Office of Basic Energy Sciences, of the U.S. Department of Energy under Contract No. DE-AC02-05CH11231. The authors thank Chenhui Zhu at beamline 7.3.3 for assistance with data acquisition.

Conflict of Interest

The authors declare no conflict of interest.

Keywords

fullerene-free, polymer solar cells, small-molecule acceptors, structurally similar, ternary solar cells

Received: May 30, 2019
Revised: June 26, 2019
Published online: July 22, 2019

[1] Z. Luo, H. Bin, T. Liu, Z.-G. Zhang, Y. Yang, C. Zhong, B. Qiu, G. Li, W. Gao, D. Xie, K. Wu, Y. Sun, F. Liu, Y. Li, C. Yang, *Adv. Mater.* **2018**, *30*, 1706124.
[2] W. Gao, T. Liu, R. Ming, Z. Luo, K. Wu, L. Zhang, J. Xin, D. Xie, G. Zhang, W. Ma, H. Yan, C. Yang, *Adv. Funct. Mater.* **2018**, *28*, 1803128.
[3] J. Sun, X. Ma, Z. Zhang, J. Yu, J. Zhou, X. Yin, L. Yang, R. Geng, R. Zhu, F. Zhang, W. Tang, *Adv. Mater.* **2018**, *30*, 1707150.
[4] W. Liu, J. Zhang, Z. Zhou, D. Zhang, Y. Zhang, S. Xu, X. Zhu, *Adv. Mater.* **2018**, *30*, 1800403.
[5] W. Gao, T. Liu, C. Zhong, G. Zhang, Y. Zhang, R. Ming, L. Zhang, I. Xin, K. Wu, Y. Guo, W. Ma, H. Yan, Y. Liu, C. Yang, *ACS Energy Lett.* **2018**, *3*, 1760.
[6] Z. Fei, F. D. Eisner, X. Jiao, M. Azzouzi, J. A. Rohr, Y. Han, M. Shahid, A. S. R. Chesman, C. D. Easton, C. R. McNeill, T. D. Anthopoulos, J. Nelson, M. Heeney, *Adv. Mater.* **2018**, *30*, 1705209.
[7] W. Gao, M. Zhang, T. Liu, R. Ming, Q. An, K. Wu, D. Xie, Z. Luo, C. Zhong, F. Liu, F. Zhang, H. Yan, C. Yang, *Adv. Mater.* **2018**, *30*, 1800052.
[8] D. Baran, T. Kirchartz, S. Wheeler, S. Dimitrov, M. Abdelsamie, J. Gorman, R. S. Ashraf, S. Holliday, A. Wadsworth, N. Gasparini, P. Kaienburg, H. Yan, A. Amassian, C. J. Brabec, J. R. Durrant, I. McCulloch, *Energy Environ. Sci.* **2016**, *9*, 3783.
[9] D. He, F. Zhao, J. Xin, J. J. Rech, Z. Wei, W. Ma, W. You, B. Li, L. Jiang, Y. Li, C. Wang, *Adv. Energy Mater.* **2018**, *8*, 1802050.
[10] W. Li, M. Chen, J. Cai, E. L. K. Spooner, H. Zhang, R. S. Gurney, D. Liu, Z. Xiao, D. G. Lidzey, L. Ding, T. Wang, *Joule* **2019**, *3*, 819.
[11] Z. Zheng, Q. Hu, S. Zhang, D. Zhang, J. Wang, S. Xie, R. Wang, Y. Qin, W. Li, L. Hong, N. Liang, F. Liu, Y. Zhang, Z. Wei, Z. Tang, T. P. Russell, J. Hou, H. Zhou, *Adv. Mater.* **2018**, *30*, 1801801.
[12] Y. Li, L. Zhong, B. Gautam, H.-J. Bin, J.-D. Lin, F.-P. Wu, Z. Zhang, Z.-Q. Jiang, Z.-G. Zhang, K. Gundogdu, Y. Li, L.-S. Liao, *Energy Environ. Sci.* **2017**, *10*, 1610.
[13] J. Yuan, Y. Zhang, L. Zhou, G. Zhang, H.-L. Yip, T.-K. Lau, X. Lu, C. Zhu, H. Peng, P. A. Johnson, M. Leclerc, Y. Cao, J. Ulanski, Y. Li, Y. Zou, *Joule* **2019**, *3*, 1.
[14] Y. Cui, H. Yao, L. Hong, T. Zhang, Y. Xu, K. Xian, B. Gao, J. Qin, J. Zhang, Z. Wei, J. Hou, *Adv. Mater.* **2019**, *31*, 1808356.
[15] Y. Chen, P. Ye, X. Jia, W. Gu, X. Xu, X. Wu, J. Wu, F. Liu, Z.-G. Zhu, H. Huang, *J. Mater. Chem. A* **2017**, *5*, 19697.
[16] Y. Chen, P. Ye, Z.-G. Zhu, X. Wang, L. Yang, X. Xu, X. Wu, T. Dong, H. Zhang, J. Hou, F. Liu, H. Huang, *Adv. Mater.* **2017**, *29*, 1603154.
[17] H. Lu, J. Zhang, J. Chen, Q. Liu, X. Gong, S. Feng, X. Xu, W. Ma, Z. Bo, *Adv. Mater.* **2016**, *28*, 9559.
[18] B. Fan, W. Zhong, X.-F. Jiang, Q. Yin, L. Ying, F. Huang, Y. Cao, *Adv. Energy Mater.* **2017**, *7*, 1602127.
[19] J. Zhang, Y. Zhang, J. Fang, K. Lu, Z. Wang, W. Ma, Z. Wei, *J. Am. Chem. Soc.* **2015**, *137*, 8176.
[20] W. Li, D. Yan, F. Liu, T. Russell, C. Zhan, J. Yao, *Sci. China: Chem.* **2018**, *61*, 1609.
[21] L. Nian, Y. Kan, H. Wang, K. Gao, B. Xu, Q. Rong, R. Wang, J. Wang, F. Liu, J. Chen, G. Zhou, T. P. Russell, A. K. Y. Jen, *Energy Environ. Sci.* **2018**, *11*, 3392.
[22] Z. Zhou, S. Xu, J. Song, Y. Jin, Q. Yue, Y. Qian, F. Liu, F. Zhang, X. Zhu, *Nat. Energy* **2018**, *3*, 952.
[23] H. Li, Z. Xiao, L. Ding, J. Wang, *Sci. Bull.* **2018**, *63*, 340.
[24] H.-H. Gao, Y. Sun, X. Wan, X. Ke, H. Feng, B. Kan, Y. Wang, Y. Zhang, C. Li, Y. Chen, *Adv. Sci.* **2018**, *5*, 1800307.
[25] Y. Xie, F. Yang, Y. Li, M. A. Uddin, P. Bi, B. Fan, Y. Cai, X. Hao, H. Y. Woo, W. Li, F. Liu, Y. Sun, *Adv. Mater.* **2018**, *30*, 1803045.
[26] X. Song, N. Gasparini, M. M. Nahid, S. H. K. Paleti, J.-L. Wang, H. Ade, D. Baran, *Joule* **2019**, *3*, 846.
[27] W. Wu, G. Zhang, X. Xu, S. Wang, Y. Li, Q. Peng, *Adv. Funct. Mater.* **2018**, *28*, 1707493.
[28] R. Yu, S. Zhang, H. Yao, B. Guo, S. Li, H. Zhang, M. Zhang, J. Hou, *Adv. Mater.* **2017**, *29*, 1700437.
[29] Z. Li, X. Xu, W. Zhang, X. Meng, Z. Genene, W. Ma, W. Mammo, A. Yartsev, M. R. Andersson, R. A. J. Janssen, E. Wang, *Energy Environ. Sci.* **2017**, *10*, 2212.
[30] L. Zhan, S. Li, H. Zhang, F. Gao, T.-K. Lau, X. Lu, D. Sun, P. Wang, M. Shi, C.-Z. Li, H. Chen, *Adv. Sci.* **2018**, *5*, 1800755.
[31] J. Lee, S.-J. Ko, M. Seifrid, H. Lee, C. McDowell, B. R. Luginbuhl, A. Karki, K. Cho, T.-Q. Nguyen, G. C. Bazan, *Adv. Energy Mater.* **2018**, *8*, 1801209.
[32] S. Dai, Y. Xiao, P. Xue, J. James Rech, K. Liu, Z. Li, X. Lu, W. You, X. Zhan, *Chem. Mater.* **2018**, *30*, 5390.
[33] L. Yang, W. Gu, L. Hong, Y. Mi, F. Liu, M. Liu, Y. Yang, B. Sharma, X. Liu, H. Huang, *ACS Appl. Mater. Interfaces* **2017**, *9*, 26928.
[34] N. Felekidis, E. Wang, M. Kemerink, *Energy Environ. Sci.* **2016**, *9*, 257.
[35] K. Jiang, G. Zhang, G. Yang, J. Zhang, Z. Li, T. Ma, H. Hu, W. Ma, H. Ade, H. Yan, *Adv. Energy Mater.* **2018**, *8*, 1701370.
[36] D. Baran, R. S. Ashraf, D. A. Hanifi, M. Abdelsamie, N. Gasparini, J. A. Rohr, S. Holliday, A. Wadsworth, S. Lockett, M. Neophytou, C. J. M. Emmott, J. Nelson, C. J. Brabec, A. Amassian, A. Salleo, T. Kirchartz, J. R. Durrant, I. McCulloch, *Nat. Mater.* **2017**, *16*, 363.
[37] M. Zhang, Z. Xiao, W. Gao, Q. Liu, K. Jin, W. Wang, Y. Mi, Q. An, X. Ma, X. Liu, C. Yang, L. Ding, F. Zhang, *Adv. Energy Mater.* **2018**, *8*, 1801968.
[38] M. Zhang, W. Gao, F. Zhang, Y. Mi, W. Wang, Q. An, J. Wang, X. Ma, J. Miao, Z. Hu, X. Liu, J. Zhang, C. Yang, *Energy Environ. Sci.* **2018**, *11*, 841.
[39] P. Cheng, J. Wang, Q. Zhang, W. Huang, J. Zhu, R. Wang, S.-Y. Chang, P. Sun, L. Meng, H. Zhao, H.-W. Cheng, T. Huang, Y. Liu, C. Wang, C. Zhu, W. You, X. Zhan, Y. Yang, *Adv. Mater.* **2018**, *30*, 1801501.
[40] B. Kan, Y.-Q.-Q. Yi, X. Wan, H. Feng, X. Ke, Y. Wang, C. Li, Y. Chen, *Adv. Energy Mater.* **2018**, *8*, 1800424.
[41] W. Su, Q. Fan, X. Guo, X. Meng, Z. Bi, W. Ma, M. Zhang, Y. Li, *Nano Energy* **2017**, *38*, 510.
[42] Z. Hu, F. Zhang, Q. An, M. Zhang, X. Ma, J. Wang, J. Zhang, J. Wang, *ACS Energy Lett.* **2018**, *3*, 555.
[43] W. Jiang, R. Yu, Z. Liu, R. Peng, D. Mi, L. Hong, Q. Wei, J. Hou, Y. Kuang, Z. Ge, *Adv. Mater.* **2018**, *30*, 1703005.
[44] T. Liu, Z. Luo, Q. Fan, G. Zhang, L. Zhang, W. Gao, X. Guo, W. Ma, M. Zhang, C. Yang, Y. Li, H. Yan, *Energy Environ. Sci.* **2018**, *11*, 3275.
[45] M. Zhang, X. Guo, W. Ma, H. Ade, J. Hou, *Adv. Mater.* **2015**, *27*, 4655.

[46] W. Zhao, S. Li, H. Yao, S. Zhang, Y. Zhang, B. Yang, J. Hou, *J. Am. Chem. Soc.* **2017**, *139*, 7148.
[47] Y. Lin, Q. He, F. Zhao, L. Huo, J. Mai, X. Lu, C.-J. Su, T. Li, J. Wang, J. Zhu, Y. Sun, C. Wang, X. Zhan, *J. Am. Chem. Soc.* **2016**, *138*, 2973.
[48] Y. Chen, X. Zhang, C. Zhan, J. Yao, *ACS Appl. Mater. Interfaces* **2015**, *7*, 6462.
[49] A. Tang, C. Zhan, J. Yao, *Adv. Energy Mater.* **2015**, *5*, 1500059.
[50] J. Lee, K. Vandewal, S. R. Yost, M. E. Bahlke, L. Goris, M. A. Baldo, J. V. Manca, T. Van Voorhis, *J. Am. Chem. Soc.* **2010**, *132*, 11878.
[51] G. Grancini, M. Maiuri, D. Fazzi, A. Petrozza, H. J. Egelhaaf, D. Brida, G. Cerullo, G. Lanzani, *Nat. Mater.* **2013**, *12*, 29.
[52] J. Mai, Y. Xiao, G. Zhou, J. Wang, J. Zhu, N. Zhao, X. Zhan, X. Lu, *Adv. Mater.* **2018**, *30*, 1802888.
[53] D. Yan, W. Liu, J. Yao, C. Zhan, *Adv. Energy Mater.* **2018**, *8*, 1800204.